

# Correlation Study of SWOT Payload Acoustic Prediction and Test

Li Lin<sup>1</sup>

*Jet Propulsion Laboratory, California Institute of Technology, Pasadena, CA, 91109, USA*

Alexis Castel<sup>2</sup>

*ESI Group, Farmington Hills, MI, 48334, USA*

Andrew Kissil<sup>3</sup>, and Gary Wang<sup>4</sup>

*Jet Propulsion Laboratory, California Institute of Technology, Pasadena, CA, 91109, USA*

Bryce Gardner<sup>5</sup>

*ESI Group, Farmington Hills, MI, 48334, USA*

Spacecraft and its payload structures are subject to severe acoustic loading during launch and ascension through the atmosphere. These harsh acoustic environments can potentially damage mission critical components and jeopardize mission success. It is well-known that high-quality vibro-acoustic predictions are vital to achieve the optimal spacecraft and payload structure designs with reduced weight. It is also widely recognized that the well-established knowledge base of damping loss factor of the structure is one of the key elements to accurately characterize and predict the structural dynamic responses under acoustic excitations. This paper focuses on assessing the influences of damping loss factor to the correlation errors between the coupled finite element/boundary element method vibro-acoustic analysis predictions and acoustic reverberation chamber test data of the Surface Water and Ocean Topography Mission Payload. The current work also aims at addressing the identification of the major sources of discrepancies, and exploration of development on the improved modal damping distribution for vibro-acoustic analysis.

## I. Introduction

The Surface Water and Ocean Topography (SWOT) Mission had been jointly developed by NASA/JPL and Centre National D'Etudes Spatiales (CNES) with contributions from other international partners. The SWOT Payload (PL) will make the first-ever global survey of the Earth's surface water, to observe the fine details of the ocean's surface topography. This mission is attained via a number of science instruments, including a Ka-band synthetic aperture radar (SAR) interferometric system (KaRIn), a conventional Jason heritage altimeter for long ocean wavelengths, and other heritage instruments such as GPS.

---

<sup>1</sup> Ph.D., Structural Engineer, Dynamics and Structures, 4800 Oak Grove Dr, Pasadena, CA 91109.

<sup>2</sup> Ph.D., Technical Manager, Aerospace Vibroacoustic, 32605 West 12 Mile Road, Farmington Hills, MI 48334.

<sup>3</sup> Principal Engineer, Dynamics and Structures, 4800 Oak Grove Dr, Pasadena, CA 91109.

<sup>4</sup> Chief Engineer, Payload & Small Spacecraft Mechanical Engineering, 4800 Oak Grove Dr, Pasadena, CA 91109.

<sup>5</sup> Ph.D., Lead Acoustic Scientist, Aerospace Vibroacoustic, 32605 West 12 Mile Road, Farmington Hills, MI 48334.

The purposes of the PL dynamic tests were to demonstrate the SWOT PL can sustain the protoflight dynamic environments, to verify the workmanship, and to provide a test verified structural model for final coupled loads analysis. As a part of the PL dynamic test campaign, the SWOT PL was subjected to the protoflight acoustic environments. Such environments are to emulate the acoustic loads induced by the rocket's launch and ascension through the atmosphere, and are deemed to be one of the most intense dynamic load environments during SWOT PL service life. Structures with relatively low surface mass density, such as radiator panels, decks, equipment panels, and antenna reflectors, are often susceptible to the severe acoustic loads faced in the launch and ascension phases. Sensitive or critical components such as sensors, thrusters, and control system units are directly attached or near to these large lightweight structures, and excessive random vibrations caused by modal and/or fluid-structure couplings can damage these components and potentially jeopardize mission success. Therefore, it is imperative to accurately predict structural responses and acoustic environments of spacecraft and its payloads during design and development phases for design optimization, risk & cost reduction, and obtaining data to support the verification & derivation of the assembly random vibration specifications.

Several vibro-acoustic analysis methodologies are adopted widely to evaluate structural integrity and/or responses under acoustic loads at any phase of the program, and can better inform the design of structures before physically building and testing. Among those tools, the coupled Finite Element/Boundary Element Method (FE/BEM) is practically attractive due to their intrinsic natures for tackling the fluid-structure interaction problem. For spacecraft and its payloads, domain-based approach such as finite element method (FEM) can predict dynamic responses of structures accurately, and is more computationally efficient, due to its ability to produce sparse matrices leading to faster solutions. The boundary element method (BEM) is based on a transformation of the differential governing equation into a boundary integral equation. This offers several important advantages over FEM for solving problems involving infinite and semi-infinite fluid domains, due to the two main merits of BEM: the potential for reduced dimensionality and inherent accuracy. Thus, the coupled FE/BEM is well-suited for carrying out spacecraft- and/or payload-level vibro-acoustic analysis to predict structural integrity and responses.

A number of ongoing efforts are present in industry to correlate analytical predictions with either Reverberation Chamber Acoustic Testing or Direct Field Acoustic Testing (DFAT) data [1] [2] [3] [4] [5]. The study presented in this paper focuses on assessing the influences of damping loss factor (DLF) to the correlation errors (CEs) between the coupled FE/BEM vibro-acoustic analysis predictions and acoustic reverberation chamber test data of SWOT PL, and addressing the identification of the major sources of discrepancies.

Utilizing Modal Strain Energy (MSE) [6] [7] [8] to distribute modal damping is a simple and computationally cost-effective approach, which is widely used in damping technology and damage detection. It can be leveraged and developed for vibro-acoustic analysis. The current work also aims at exploration of development on improved modal damping distribution for vibro-acoustic analysis.

For this correlation effort, the vibro-acoustic analysis predictions were mainly compared to accelerometer test measurements in terms of overall root mean square (RMS) for all the available channels. For some channels, Power Spectral Density (PSD) results were also examined to better understand dynamic behaviors. Commercially available vibro-acoustic analysis software, VA One version r2019 [9], was used to perform the coupled FE/BEM vibro-acoustic modeling and analysis, and MSC NASTRAN (version r2019) [10] was employed to generate modal results. GraphPad Prism version 9 [11] was applied to process correlation errors.

## II. Reverberation Chamber Acoustic Testing

### A. Test Configuration

The Payload was in its full flight configuration with the exception of the star tracker mass mockups (will be added by Thales in France before Observatory-level dynamic tests) and the Nadir deck MLI. Figure II-1 shows the configuration of the SWOT Payload in the ETL acoustic chamber. The PL was placed in the center of the acoustic chamber and the rotated by 22 degrees about its vertical axis. The Payload was attached to its transportation cart which was elevated from the ground using wood blocks.



**Fig. II-1 SWOT Payload Configuration in Acoustic Chamber**

#### **B. Test Instrumentation**

A series of microphones were located around the SWOT PL to measure the Sound Pressure Level (SPL) including control, monitor and response microphones to ensure the acoustic field in the chamber met the test requirements within tolerance. The locations of all microphones as tested is shown in Figure II-2.

The test article was instrumented with more than 50 triaxial and single axis accelerometers encompassing the entire SWOT PL structure to measure the acceleration spectral density (ASD) during the test. As an example, a triaxial accelerometer mounted on Top Deck Center is shown in Figure II-3.

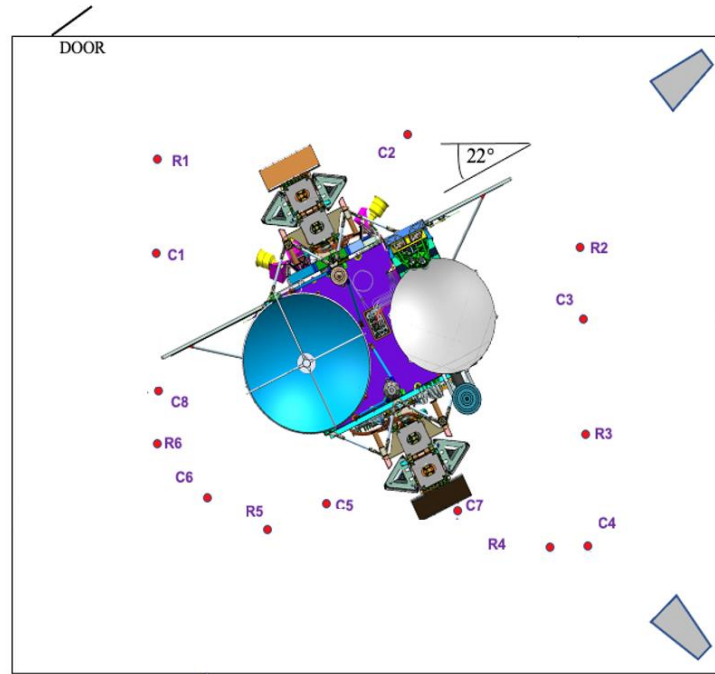


**Fig. II-2 Microphone Locations**

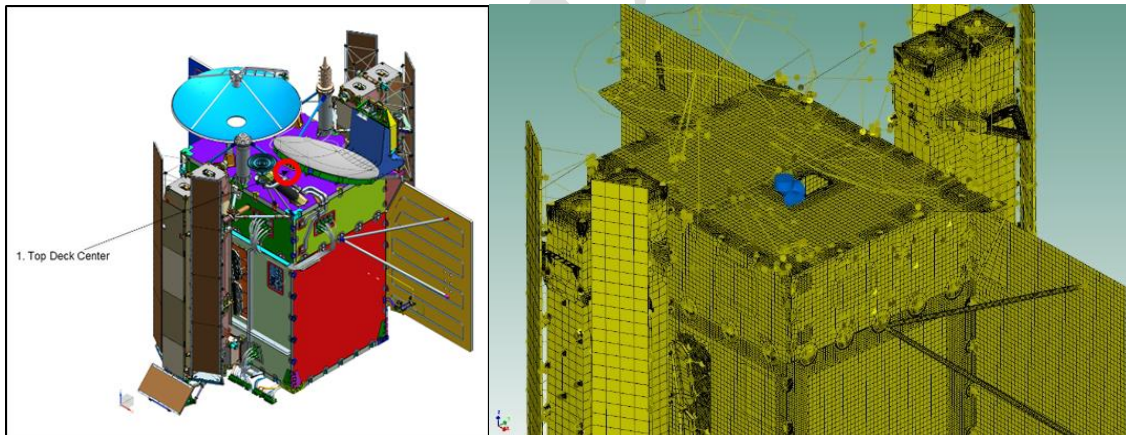


**Fig. II-3 Top Deck Center Accelerometer Location**

### C. Test Input Level

The acoustic input, shown in Figure II-4, was derived from the acoustic environment produced in a typical launch vehicle fairing during launch. During the acoustic tests, the individual control microphone measurements were input to the controller to achieve the desired acoustic levels within a specified tolerance.



**Fig. II-4 PL Acoustic Level Requirement**

### III. Pre-Test Analysis and Initial Comparison to Test Data

#### A. Pre-Test Modeling and Analysis

The FE/BEM vibro-acoustic analysis requires a structural finite element (FE) model to couple with a boundary element (BE) model for computing the dynamic responses of structure to an acoustic loading.

First, the PL FE model (as shown in Figure III-1) that had been test-correlated up to 50Hz in a separate development test model (DTM) modal survey effort, was adapted to provide the dynamic characteristics of the test article (TA). There are about 750K nodes in the PL FE model. It is considered a high-fidelity model for a system-level dynamic test structures model. The PL FE model was attached to a transportation cart via 4 corner adapters, the cart rested on wood blocks. Note that the MGSE (including cart, adapters, and wood blocks) was condensed to a Direct Matrix Input at Grid points (DMIG) for reducing model size, and it was not expected to be acoustically susceptible. TA FE model (i.e. PL FE model plus DMIG of MGSE) was fixed at MGSE to the ground interface. In order to capture all dynamic influences to the vibro-acoustic analysis, the fixed-base TA modal analysis was run up to 600Hz containing more than 2300 modes.

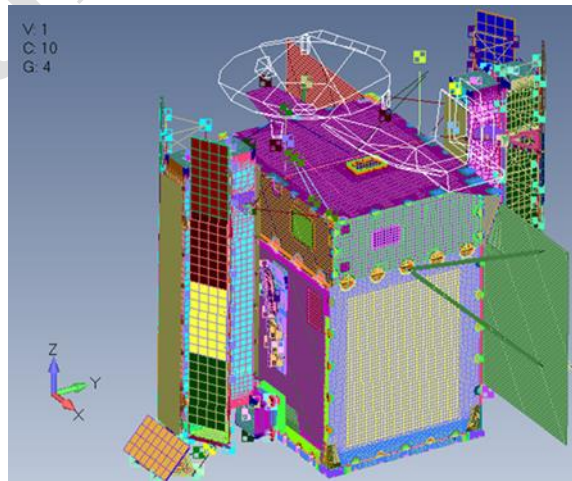


**Fig. III-1 PL FE Model**

Secondly, the exterior boundaries of the SWOT PL that are susceptible to acoustic loads, were discretized for BE meshing. Despite its advantages, BE analysis can be computationally expensive, which stems from its global nature. That is, the boundary integral equation formulation generally specifies the global interactions among sources, objects and fields, which usually leads to a dense matrix equation after discretization. Consequently, fewer nodes are desired to represent a typical surface than in the FE model. PL BE mesh (as shown in Figure III-2) has about 4500 nodes. The maximum element size is based on 6 elements per wavelength, at the highest BEM solution frequency of 500Hz. The BE mesh represents fluid-structure interface in the coupled FE/BEM vibro-acoustic analysis. With such an interface, the FE structural modes are projected onto the BE mesh if FE and BE have incompatible meshes, and FE structure will have effects on the fluid field. The acoustic excitation on all surfaces of the BE model was assumed to be a stationary random diffuse field and discretized as equally spaced uncorrelated plane waves. A baseline (BL) structural damping loss factor (DLF) 2%, or 1% critical damping was applied for all structural modes in the pre-test vibro-acoustic analyses, based on the recommendations from the similar size of structure [1].

In order to effectively and accurately predict dynamic behavior of SWOT PL under acoustic inputs, rigorous convergence studies were conducted including BE mesh locations & fidelity, number of plane waves, BEM frequency resolutions and solution frequency ranges. Consequently, 1/24<sup>th</sup> octave frequency resolution and 50 equally spaced plane waves were utilized for the PL BL model (i.e. 2% DLF).

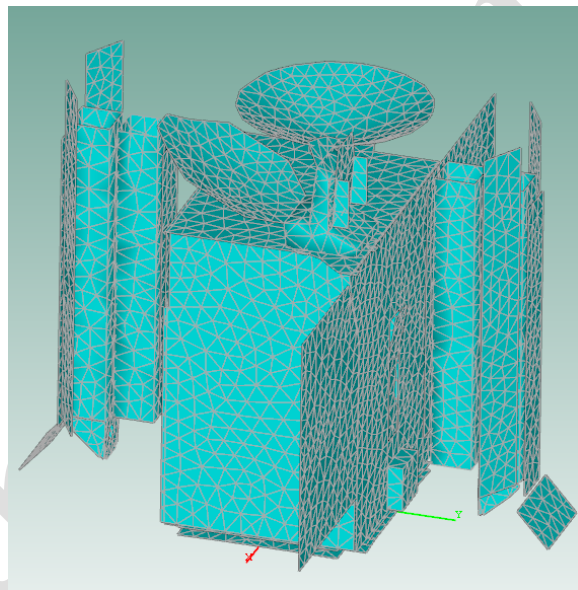


**Fig. III-2 PL Boundary Element Model**

#### **B. Initial Comparisons Between Analysis and Test Data**

As the first step of test and analysis correlation effort, the results of SPL, RMS and PSD from the PL BL model were directly compared to the reverberation chamber acoustic test data. The baseline vibro-acoustic prediction for the SPL at the randomly selected control microphone location is shown in Figure III-3, where the measured data and analytical prediction are compared on 1/3<sup>rd</sup> octave band and overlaid by the acoustic input specification profile. The VA One's prediction in most of the 1/3<sup>rd</sup> octave bands are within 3dB and with less than 4dB deviations on frequency bands over 25Hz and 500Hz. These are deemed to be acceptable given the individual control microphone variations seen during acoustic tests as compared to the acoustic input level applied in the FE/BEM vibro-acoustic analysis. Figure III-4 illustrates the comparison of RMS for all the available channels, and Figure III-5 presents PSD comparison of FE/BEM analysis prediction to the measured data at randomly selected channels.

The vibro-acoustic prediction (per BL 2% DLF) seemingly captures the spread in RMS, SPL and PSD fairly well. Nevertheless, further analysis and study were needed to quantitatively evaluate DLF effects on correlation between prediction and test data.

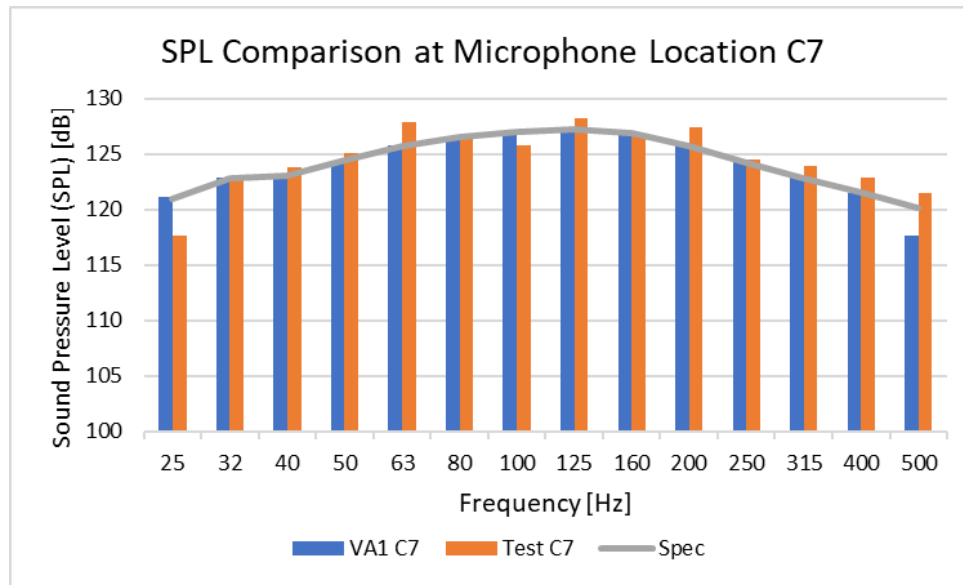


**Fig. III-3 SPL Comparison Around PL for BL Model**

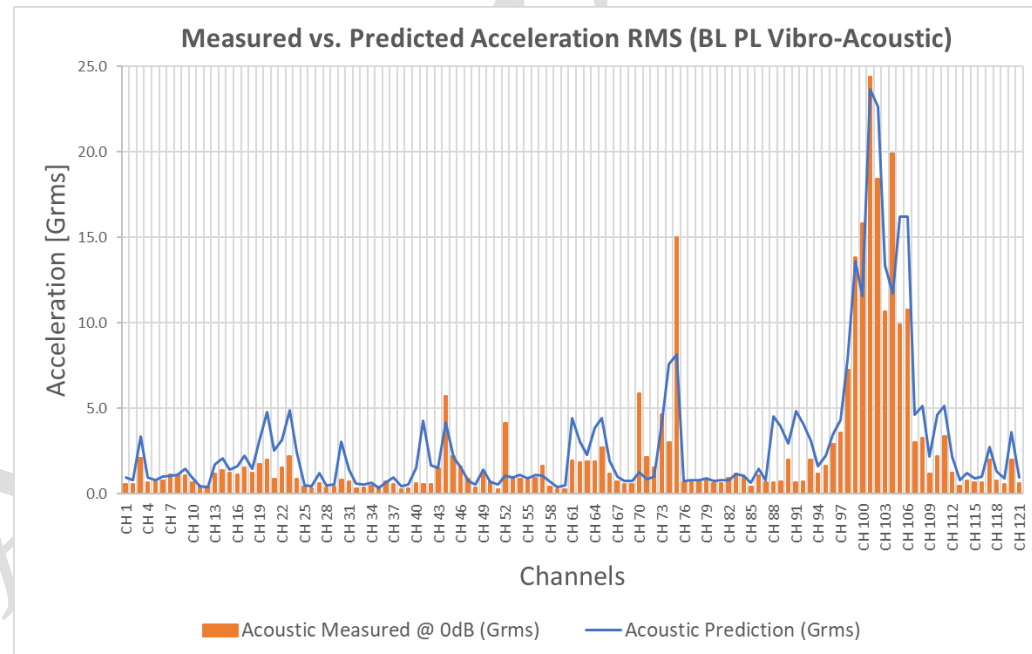


**Fig. III-4 Comparison of RMS for All Channels: PL BL Prediction to Test**

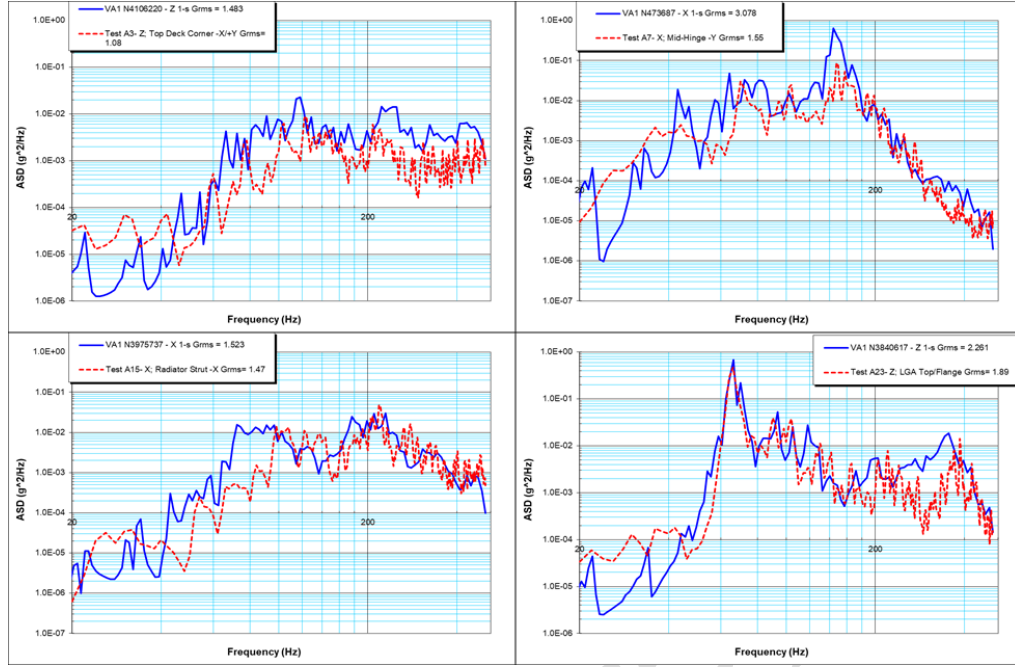


**Fig. III-5 PSD Comparison at Randomly Selected Channels (PL BL)**

#### IV. Post-Test Analysis and Correlation Study

##### A. Post-Test Modeling and Analysis

To evaluate damping effects on dynamic responses at test accelerometer locations, DLF was traded for values of 1% and 3% in the PL vibro-acoustic model. Comparison studies for various BEM octave frequency resolutions (e.g. 1/24<sup>th</sup>, 1/36<sup>th</sup> and 1/42<sup>nd</sup> octaves, etc.) were carried out to make sure capturing narrow-band response peaks with all damping assumptions. RMS values of all the available channels were evaluated side-by-side for the various octave cases. Comparisons of RMS between 1/24<sup>th</sup> and 1/36<sup>th</sup> octaves for 1% DLF cases are presented in Figure IV-1. 9 out of 130 channels have 10% to 25% discrepancies in terms of overall RMS.

Based on the post-test convergence studies, 1/36<sup>th</sup> octave was chosen for 1% DLF case and 1/24<sup>th</sup> octave was used for 3% DLF case. For this work, high modal density alleviates risk on missing peaks when using relatively coarse octave frequency resolution (i.e., 1/24<sup>th</sup> octave). Computational time of 1/24<sup>th</sup> octave was reduced by about 40% compared to using 1/36<sup>th</sup> octave for the same case. There were only negligible differences between 1/36<sup>th</sup> octave and 1/42<sup>nd</sup> octave for all cases in terms of overall RMS values.

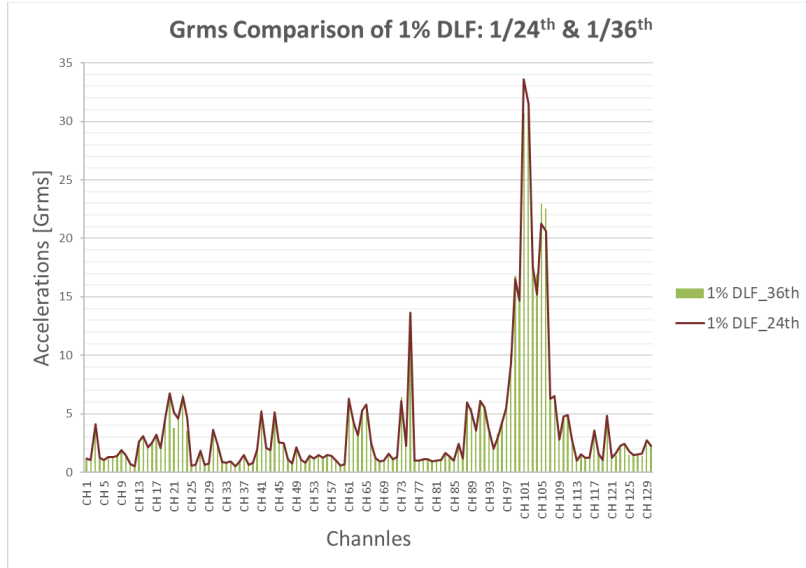


**Fig. IV-1 Comparison of RMS for Various Octaves: 1% DLF**

### B. Brief Discussion of Damping Loss Factor in Vibro-Acoustic Analysis

When a structure is vibrating due to fluid mediums which act as force excitations, the total loss factor exhibited in this structure can be expressed as

$$D_t = D_{struct} + D_{rad} \quad (\text{IV-1})$$

where  $D_{struct}$  is the structural loss factor.  $D_{rad}$  is the radiation loss factor, which is defined as ratio of radiated sound energy to the vibrational energy of the structure. Radiation loss factor is from the radiation of sound as a result of the fluid-structure interaction. It is commonly understood that vibro-acoustic FE/BEM analyses are very sensitive to the damping loss factor. For complex structures, the efficient way is to characterize the DLF from test and prediction correlations. In VA One, user can specify the structural damping. The software takes care of the fluid-structure interaction terms by internally computing the modal impedance matrix, which contains the acoustic interactions between the fluid and the structure as well as radiation damping and fluid loading to the structure. BEM solver provides a fully coupled modal damping matrix and a fully coupled modal mass matrix for the fluid.

### C. Correlation Approach

RMS values of test data were based on the “default” 20 – 2000Hz, and were up to the maximum analysis frequency of 500Hz for the predictions.

For each of the 54 measurement locations that were used for correlation, all measured directions were compared, respectively.

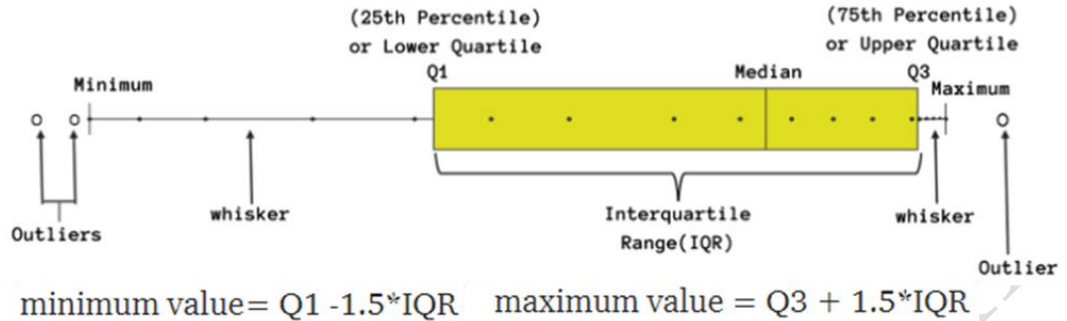
All of the accelerometers were placed into two groups (i.e. “Struct” and “Simple”) according to the dynamic modeling fidelities of the surrounding structures where the accelerometers were mounted. Furthermore, all of the accelerometers were categorized per the type of structure, type of modeling, and location.

Correlation error, as defined in Eq. (2), was applied to all of the RMS results for all 3 DLF cases. Note that the positive CE values mean over-predictions, whereas negative values indicate under-predictions.

$$CE(\text{dB}) = 20 \log_{10} \frac{RMS_{Predict}}{RMS_{test}} \quad (\text{IV-2})$$

Box Plot (or Box-Whisker Plot) was used for visualizing correlation results in statistical perspective. Such plot can show distribution & shape of the data, median, maximum and minimum values, and it allows for quick side-by-side

comparisons between groups. Note that statistical summaries, i.e. median and interquartile range, are robust to outliers and skewness. An example of Tukey style plot is illustrated in Figure IV-2.



<https://medium.com/mlpoint/box-plot-box-and-whiskers-plot-what-does-it-tell-you-99e827fac158>

**Fig. IV-2 Example of Tukey Box-Plot**

Three types of Box Plot were leveraged, i.e. Min & Max with all points; 5<sup>th</sup> & 95<sup>th</sup> percentiles; and Tukey (25<sup>th</sup> & 75<sup>th</sup> percentiles), for various purposes. Also, median (50<sup>th</sup> percentile) and mean (as “+”) were included on each plot.

#### D. Correlation Results

Figure IV-3 shows the prediction to test CEs for all of the 130 channels for each DLF case. Note that 100% of the data were contained between the whisker ends. Data values were superimposed on the box plots to aid in visualization. Center lines show the medians. One may find that 2% DLF and 3% DLF cases yielded better correlations. This finding can be augmented by Table IV-1.

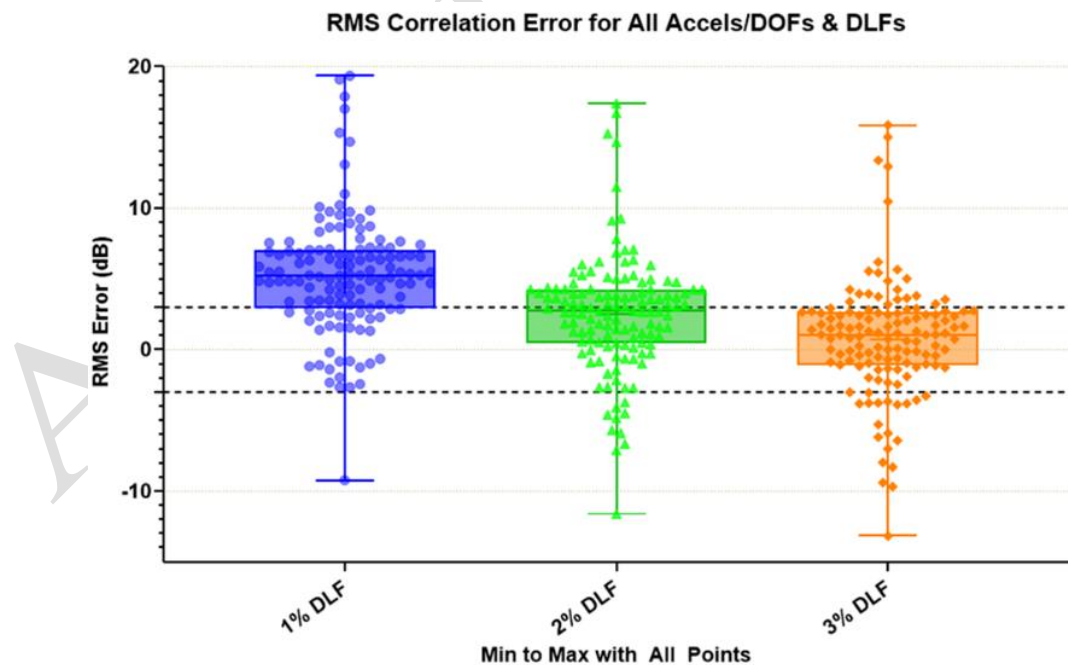


**Fig. IV-3 All CE Data Plotted as a Group for Each DLF Case**

**Table IV-1 CEs Classed per Tolerances for Each DLF Case**

	1% DLF	2% DLF	3% DLF
within +/- 3dB			
<b>Total</b>	<b>25.4%</b>	<b>44.6%</b>	<b>66.9%</b>
< 0dB	10.8%	13.1%	22.3%
0 - +3dB	14.6%	31.5%	44.6%
within +/- 2dB			
<b>Total</b>	<b>12.3%</b>	<b>30.0%</b>	<b>46.2%</b>
< 0dB	7.7%	9.2%	20.0%
0 - +2dB	4.6%	20.8%	26.2%

CEs per “Struct” and “Simple” groups for all DLF cases are presented in Figure IV-4. For the same data sets: Tukey Box Plot (on the left side) offers a quick detection of outliers; On the right side, extending the whiskers to the 5<sup>th</sup> and 95<sup>th</sup> percentiles of the data will capture 90% of the data within the whisker ends, which reflects the standard 95% confidence level. Results show that CE medians of “Struct” and “Simple” are 0dB and 2.3dB, respectively, for 3% DLF case. Overall, 3% DLF predictions are slightly closer to 0dB correlation error than 2% DLF results.

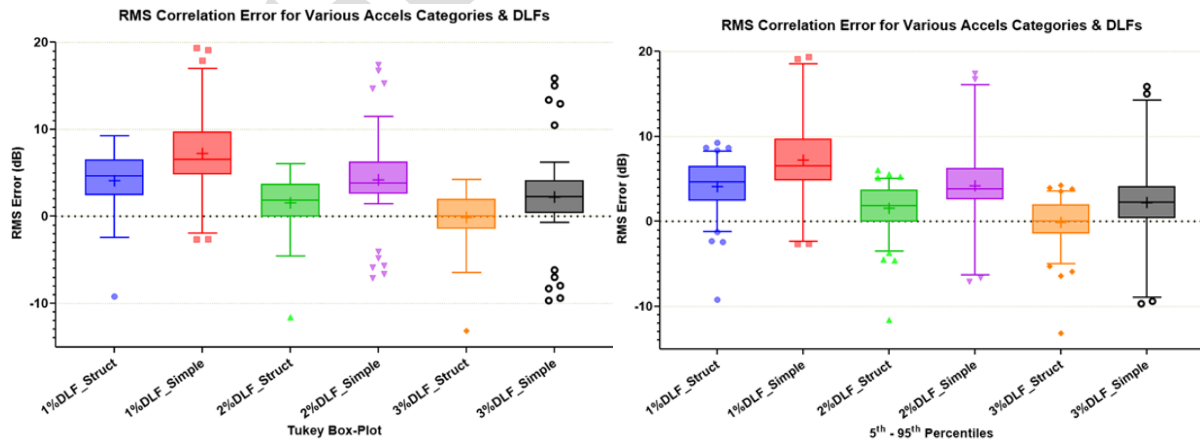


**Fig. IV-4 CEs per “Struct” & “Simple” Groups for Each DLF Case**

Generally good correlations could be expected from the predictions of the structures that are modeled with adequate dynamic behaviors. Figure IV-5 shows the CEs for this category. As one can see that the median is 0.9 dB

for 3% DLF case. If plotted in Tukey style, no outlier was identified. Considerably good correlations of PSD are indeed observed in Figures IV-6 and IV-7.

Joints are seldom modeled in sufficient detail in system level dynamic FE models. Figure IV-8 represents the CEs from the category of accelerometers which were next to loose joints. The structures that those accelerometers were mounted to, were well-modeled. However, the nearby joints with large clearances caused the outliers are as low as -11dB & -13dB for 2% & 3% DLF cases, respectively. PSD comparison (Figure IV-9) shows that the predictions deviate from test data starting 200Hz for the selected channel.

Large surface structures like Antenna Reflector, Radiator Panels and Solar Array Panels typically exhibit relatively low surface density and primary mode, and can be appreciably excited by the acoustic waves and fluid-structure interactions induced vibrations. Good correlations can be anticipated from such structures if modeled properly, as shown in Figure IV-10. However, if accelerometers are mounted to large surface structures with insufficiently modeled dynamic characteristics, more scattered correlation error could be yielded. Figure IV-11 illustrates the accelerometer attached to the PL base panel, in between two large boxes. The large boxes were represented by RBEs and point masses, so the dynamic interactions among panel, large components, cable and harnesses were not captured in this system-level FE model. The unsatisfactory correlation errors can be seen on this plot.

Often times, mechanisms and interfaces are simplified due to size limit of system-level dynamic model. Consequently, poor correlations would exist for these areas. Figure IV-12 shows the accelerometers that were mounted to Mid-Hinge mechanism, which is a hinge joint with actuation. This mechanism was modeled using point mass, rigid and spring elements in the system level FE model, and less damped responses were produced by such simplifications. Correlation errors can be greater than 5dB in terms of both mean and median per 3% DLF case, and Box-Whisker plots are showing little overlaps among 3 damping loss factor cases.

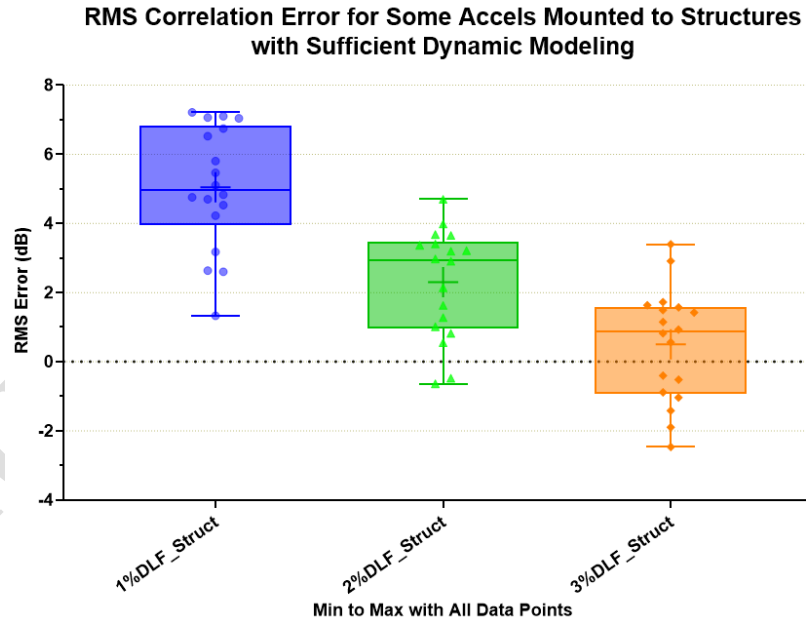


**Fig. IV-5 CEs for Category of Adequately Modeled Dynamics**

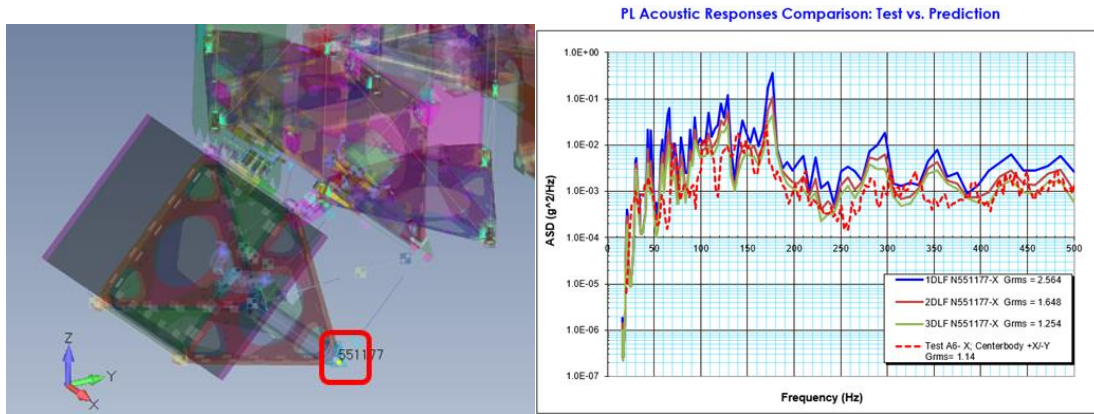


**Fig. IV-6 PSD Comparison of an Accelerometer Mounted to Structure with Amply Modeled Dynamics**

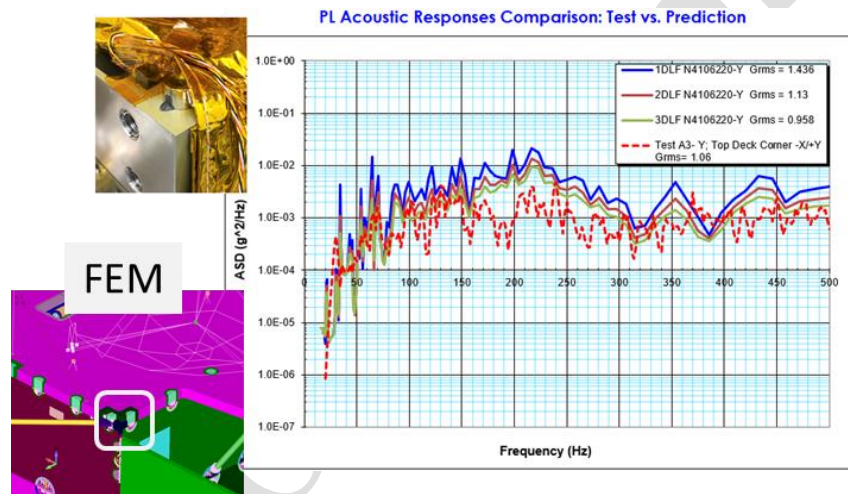


**Fig. IV-7 PSD Comparison of an Accelerometer Mounted to a Suitably Modeled Large Surface**

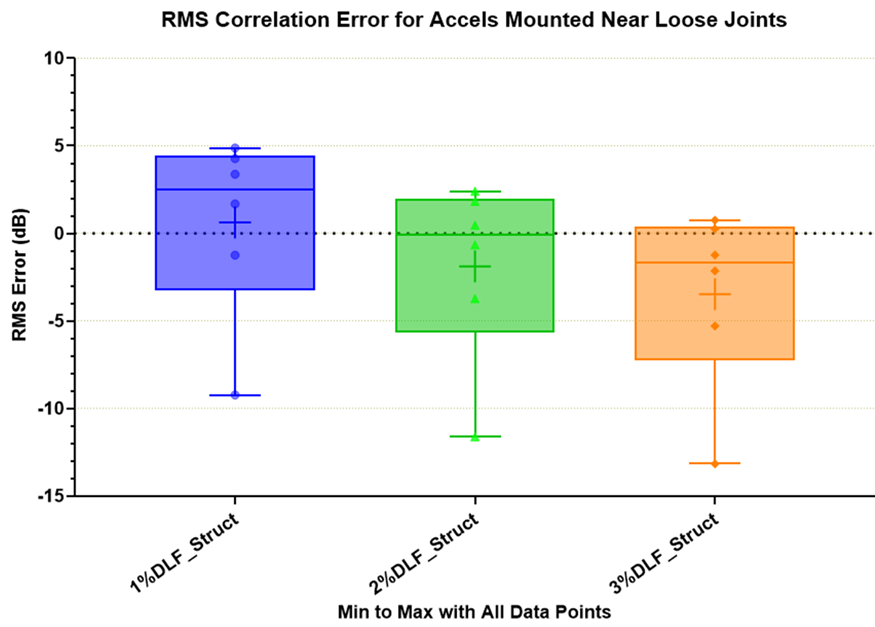


**Fig. IV-8 CEs for Category of Accelerometers Near to Loose Joints**

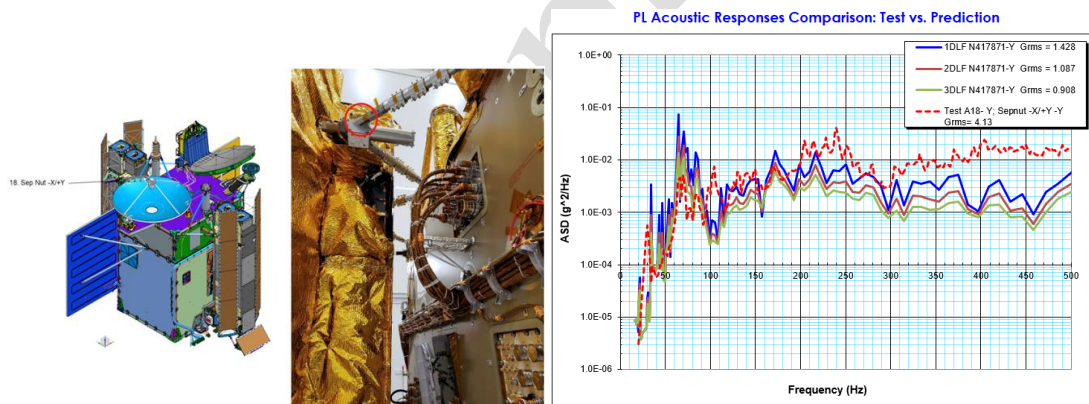


**Fig. IV-9 PSD Comparison of an Accelerometer Near to Loose Joint**

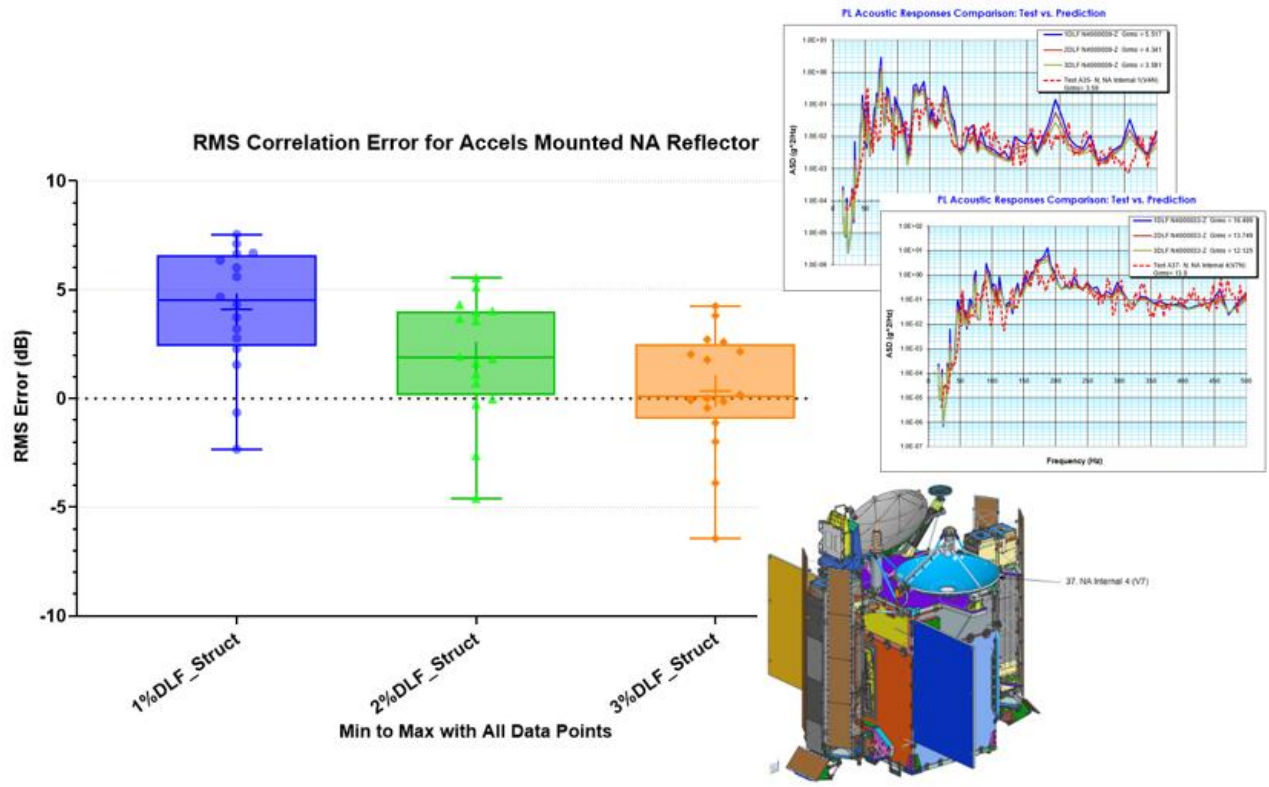


Fig. IV-10 CEs from Accels Mounted on Properly Modeled Antenna Reflector

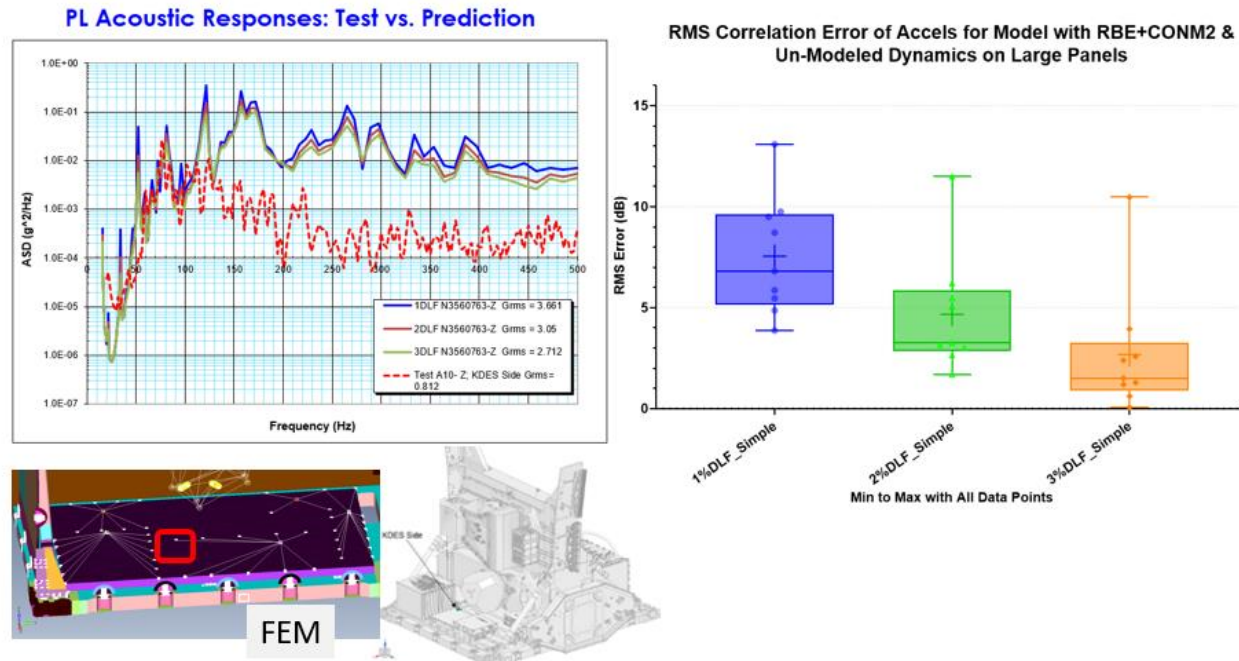
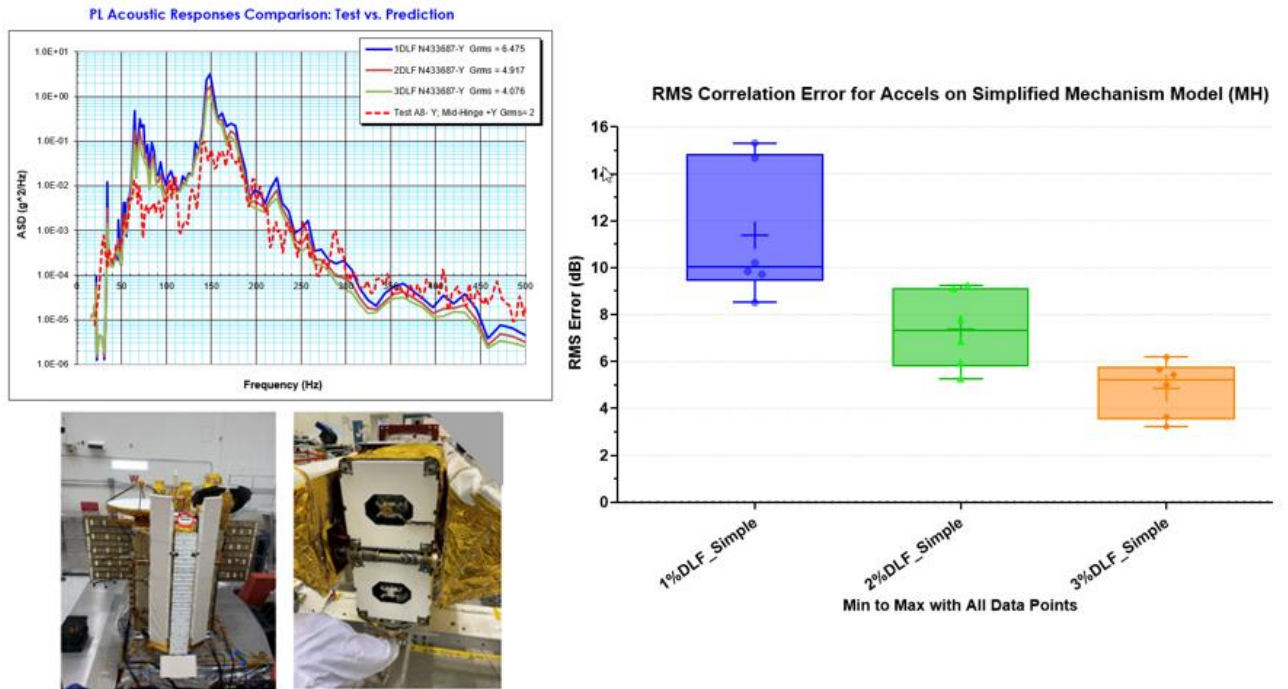


Fig. IV-11 CEs from Accels Mounted on Panels with Un-modeled Dynamics



**Fig. IV-12 CEs from Accels Mounted Near to Mechanism**

## V. Correlation Study with Enhanced Modal Damping Distribution

### A. Development of Modal Damping Distribution

Traditionally, modal frequency response solutions have limited damping modeling options. As damping must be expressed on a modal basis, the two most convenient ways of accounting for damping in a simulation model are:

- to assume the damping uniform throughout the model or import a modal damping matrix,
- to project from the stiffness matrix as the normal mode analysis is performed by the finite element solver.

For uniform damping, if the modal dynamic stiffness matrix is noted as  $\mathbf{D}_{tot}$ , the structural damping is then written as

$$\mathbf{D}_{loss}(\omega) = \eta(\omega) \mathbf{K}_{modal} \quad (V-1)$$

note that here the applied damping may be frequency-dependent. This is key as on industrial structures experimental data tends to show that damping decreases as the frequency range increases.

Similarly, for the second option identified above, we can identify  $\mathbf{D}_{loss}$  as a quantity proportional to the imaginary part of the stiffness matrix  $\mathbf{K}$  assembled by the finite element solver; in this case, we have

$$\mathbf{D}_{loss} = \mathbf{P} \operatorname{Im}(\mathbf{K}_{nodal}) \mathbf{P}^T \quad (V-2)$$

with  $\mathbf{P}$  a matrix made of the mode shapes stacked together (eigenvectors). Although this second option has the advantage of allowing for a non-uniform damping distribution throughout the structure, the nature of standard modal analyses does not allow for a frequency dependence in  $\mathbf{D}_{loss}$ .

NASA Standard MSFC-STD-3676b establishes a generic damping schedule for space structural dynamics models. In this document, the proposed damping schedules for launch vehicles on Table III vary based on the frequency range and the type of panel modeled (bare panel, panel with bolt-on equipment, and panel with both bolt-on equipment and blankets). Although that particular damping schedule may not be directly applied to payload analysis such as the one discussed in this paper, this shows the need to assert damping both as a function of frequency and a function of space (i.e. some subsystems may have different damping schedules from one another).

Over the years, commercial software solutions have implemented alternative approaches to cater to this need and offer both the spatial non-uniformity and frequency dependence to model that damping into the structure. The damping distribution on the modal basis can be challenging as the  $\mathbf{K}$  matrix used in equation ( V-2 ) is typically not available as the software is performing a modal frequency response. Commercial simulation solutions like VA One currently offer the ability to spatially distribute frequency-dependent damping based on the kinetic energy of subsystems by considering the mass matrix  $\mathbf{m}_m$  of each  $m$  subsystem. We then have

$$\mathbf{D}_{loss}(\omega) = [i\eta_s \omega_{n,s}^2] \text{ with } \eta_s = \frac{\sum_{\text{FE Subs},m} \eta_m \mathbf{P}_s^T \mathbf{m}_m \mathbf{P}_s}{\sum_{\text{FE Subs},m} \mathbf{P}_s^T \mathbf{m}_m \mathbf{P}_s} \quad (\text{V-3})$$

for modes and subsystem  $m$ . (note that  $\mathbf{D}_{loss}(\omega)$  is diagonal here). The validity of this assumption relies on the fact that it is expected for the kinetic energy to be proportional to the strain energy. Validation studies have shown that this assumption is valid when subsystems have a large number of modes. However, it typically finds its limitation when damping is hyper-localized on a model and greater care must be taken when projecting damping on a modal basis.

For this study, to project non-spatially uniform frequency dependent onto the modal basis with full accuracy, a new method distributing the damping proportionally to the modal strain energy is proposed. The method can then evaluate frequency-dependent modal damping distributed similarly to the projection done by the finite element solver. With this, the diagonal terms of  $\mathbf{D}_{loss}$  are equal to those obtained by the finite element solver for a given frequency. The proposed formulation is then written as

$$\mathbf{D}_{loss}(\omega) = [i\eta_s(\omega) \omega_{n,s}^2] \text{ with } \eta_s(\omega) = \frac{\sum_{\text{FE Subs},m} \eta_m(\omega) \mathbf{E}_{s,m}^{\varepsilon}}{\sum_{\text{FE Subs},m} \mathbf{V} \mathbf{E}_{s,m}^{\varepsilon}} \quad (\text{V-4})$$

and  $\mathbf{V} \mathbf{E}_{s,m}^{\varepsilon}$  is the total strain energy of modes and subsystem.

This formulation is a major improvement to the currently available options, as now a rigorous strain energy-based distribution can be projected on a modal basis without the need for the nodal stiffness matrix. Finite element solvers typically output the modal strain energy on a per-element basis. However, considering the large amount of data and that one may want to define damping on a per subsystem basis, we can instruct the finite element solver to calculate  $\mathbf{V} \mathbf{E}_{s,m}^{\varepsilon}$  for each subsystem.

## B. Validation against finite element solver projection

As mentioned above, finite element solvers are typically able to project structural damping on a modal basis per equation ( V-2 ). When using the proposed method and setting  $\eta_m(\omega)$  to be constant as a function of the frequency, we get the same values of  $\mathbf{D}_{loss}(\omega)$  for equations ( V-2 ) and ( V-4 ).

For this, we propose studying a simple cube academic structure made of 3 different parts with each a unique damping value attached to it as shown in Figure V-1.

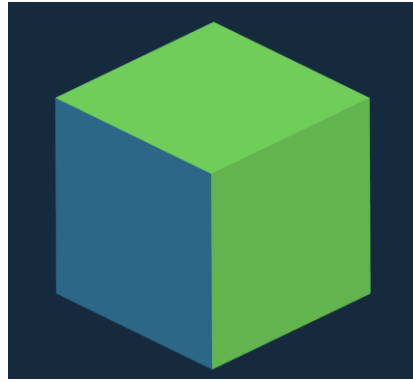


**Figure V-1 - Example of academic structure for implementation validation**

For this the finite element solver, in this case, ESI's Virtual Performance Solution (VPS) will calculate the diagonal modal damping using equation ( V-2 ). Structural damping is set to 2% for Part 1, 4% for Part 2, and 6% for Part 3. As VPS happens to automatically output the share modal strain energy per part in its output file (shown in Figure V-2) and therefore, the implementation of equation ( V-4 ) can easily be verified.

```

2668 *** INFO *** EIGEN MODE NO.      10
2669      TRANSLATIONAL SCALING FACTOR = 1.4134E-01
2670
2671
2672      SOLUTION AT EIGEN MODE NO. 10
2673 ****
2674      EIGEN FREQUENCY..... 1.4837E+01
2675      INTERNAL ENERGY..... 4.3452E+03
2676      EXTERNAL WORK..... 0.0000E+00
2677      TOTAL ENERGY..... 4.3452E+03
2678      SOLID HOURGLASS ENERGY..... 0.0000E+00
2679      SHELL HOURGLASS ENERGY..... 0.0000E+00
2680      CONTACT SPRING WORK..... 0.0000E+00
2681      CONTACT FRICTION ENERGY..... 0.0000E+00
2682      CONTACT DAMPING ENERGY..... 0.0000E+00
2683
2684      INTERNAL HOURGLASS TOTAL
2685      PART ID ENERGY ENERGY ENERGY
2686      3 24.69 % 0.00 % 24.69 %
2687      1 12.11 % 0.00 % 12.11 %
2688      2 63.20 % 0.00 % 63.20 %
2689      TOTAL 4.35E+03 0.00E+00 4.35E+03
2690
2691

```

**Figure V-2 VPS Modal Analysis output file**

Results presented in Table V-1 are used to validate the implementation, here we can see that column 3 results are equal to those of column 7. Although not shown here, the same trend continues for all verified modes.

**Table V-1 - Modal damping calculation verification**

Mode #	Frequency [Hz]	VPS Solver Calculated Modal Damping (eq. ( V-2 ))	Part ID			Calculated Damping (eq. ( V-4 ))
			1	2	3	
			Damping on part			
7	7.90	5.85%	1.54%	4.38%	94.09%	5.85%
8	8.82	5.78%	2.23%	6.75%	91.02%	5.78%
9	12.71	4.02%	11.29%	76.20%	12.51%	4.02%
10	14.84	4.25%	12.11%	63.20%	24.69%	4.25%

### C. Correlation Study Based on Improved Modal Damping Distribution

The SWOT PL Acoustic Test can now be compared to vibro-acoustic analysis results per the enhanced modal damping distribution method. Figure V-3 shows the Correlation Error comparison for Strain-Energy (SE) damping

loss factor, for uniform damping values of 2% and 3%. We see here that, as expected, the strain energy formulation results are very similar to the uniform damping results with a moderate, yet noticeable improvement over the traditional damping formulation.

Figure V-3

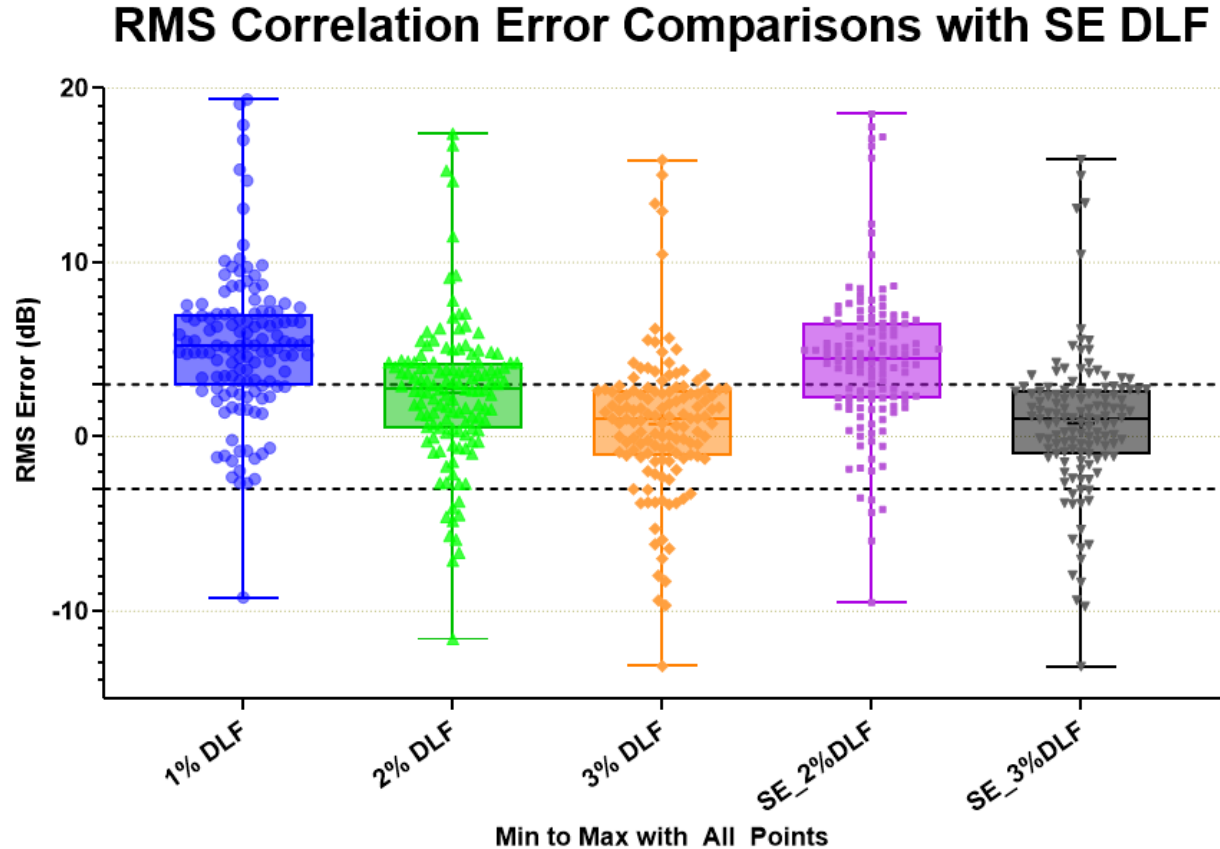


**Figure V-3 – All CE Data Plotted as a Group for the Strain Energy (SE) damping vs traditional uniform damping.**

As this correlation study was being carried out and the proposed SE damping distribution formulation lifted the classic damping definition limitations, the lack of available reference damping information (similar to what [12] offers for launch vehicles) was apparent. At the time of writing this paper, there was no way to be able to distinguish structural definition discrepancies from the finite element model from discrepancies in the definition of the damping loss factor. Therefore, additional experimental studies are necessary to evaluate damping loss factor spectra for payload structural components, potentially offering generic damping loss factor schedules for payload components.

## VI. Conclusion and Future Work

Actual damping is frequency and location/material dependent for such complex structure. If applicable, the damping values from modal survey should be leveraged to improve the accuracy of predictions. For large panels, which could be acoustically susceptible, it is desired to capture their dynamic characteristics as much as possible, for better correlations. For system-level FE model, components and subsystems are often simplified by lower fidelity elements. Less damped responses should be expected from such locations and/or elements, i.e. real hardware would exhibit more complex dynamic interactions and responses. Joints, interfaces and some mechanisms are prohibitively expensive to model in details in system level FE model. They could produce the large correlation errors. Panel mounted large components that are sometimes represented by point masses with rigid element connections, their large scattering errors could be due to omitting dynamic interactions between panel & units.

For SWOT PL-Like Structure, 2.5% DLF would be a good starting point based on correlation study done by far. However, understanding the dynamic model is more important. With more correlation data on this aspect, it would be expected to have a more realistic DLF for the vibro-acoustic analysis.

The constant DLF definition of SWOT-like PL (or S/C) Structures has a somewhat negative impact to CEs, it indicates that the subsystems may have disparate damping characteristics. There is a need of assigning various damping for different structural property groups per mode.

The Enhanced Modal Damping Distribution proposed in V lifts all restrictions related to the distribution of modal damping, keeping the full accuracy from the projection done by finite element solvers while allowing the user to define a frequency dependent damping. However, it was found during the correlation study that, although all mathematical restriction are lifted, the available damping information is limited. For launch vehicle structures, NASA standards provide generic damping schedules than can directly be used with the proposed method. In the absence of available damping information, one must exert judgement and determine whether the observed differences between test and simulation can be attributed to damping.

### Acknowledgments

The research was carried out at the Jet Propulsion Laboratory, California Institute of Technology, under a contract with the National Aeronautics and Space Administration (80NM0018D0004).

Special thanks to SWOT Dynamics Environments Team and ETL SWOT Test Team.

### References

- [1] P. Blelloch, A. M. and J. Canal, "Test Analysis Comparison for a Spacecraft Direct Field Acoustic Test," in *Spacecraft and Launch Vehicle Dynamics Environments Workshop (SCLV)*, 2015.
- [2] P. Marshal, T. McQuigg, D. Inoyama, T. Stoumbos and R. Kapania, "Acoustic Analysis of Spacecraft Cavities using the Boundary Element Method," in *AIAA Scitech 2019 Forum*, 2019.
- [3] A. Castel, A. Medeiros, B. Gardner, C. Musser, I. D. and T. Stoumbos, "Enhanced DFAT simulation: optimization and correlation study," in *Spacecraft and Launch Vehicles Dynamics Workshop (SCLV)*, 2019.
- [4] W. Ben Tsoi, A. R. Kolaini and B. W. Childs, "Vibration on Composite Reflector: Test versus Prediction," in *Spacecraft and Launch Vehicle Dynamic Environments Workshop (SCLV)*, 2008.
- [5] G. Rodrigues, "Correlation of FEM/BEM Vibroacoustic Prediction to System-level Acoustic Test Results," in *SSMET 2014 -13th European Conference on Spacecraft Structures, Materials & Environmental Testing*, 2014.
- [6] E. Ungar and E. Kerwin, "Loss factors of viscoelastic systems in term of energy concepts," *Journal of Acoustical Society of America*, vol. 34, no. 7, p. 954–957, 1962.
- [7] M. Tsai and K. Chang, "A study of the modal strain energy method for viscoelastically damped structures," *Journal of the Chinese Institute of Engineers*, vol. 24, no. 3, 2001.
- [8] F. Cura, A. Mura and F. Scarpa, "Modal strain energy based methods for the analysis of complex patterned free layer damped plates," *Journal of Vibration and Control*, vol. 18, no. 9, 2011.
- [9] VA One, *vibro-acoustic analysis software*, Paris, France: ESI Group, , Version 2019.
- [10] MSC NASTRAN, *multidisciplinary structural analysis software*, Irvine, CA: MSC Software (HEXAGON), version 2019.0.
- [11] GraphPad Prism, *statistical analysis software*, version 9, San Diego, CA: GraphPad Software, 2022.
- [12] M. S. F. C. NASA, "MSFC-STD-3676b: Development Of Vibroacoustic And Shock Design And Test Criteria," 17 03 2017. [Online]. Available: <https://standards.nasa.gov/standard/msfc/msfc-std-3676>.

Author preprint